Resonant-state expansion applied to planar open optical systems

M. B. Doost, W. Langbein, and E. A. Muljarov*
School of Physics and Astronomy, Cardiff University, Cardiff CF24 3AA, United Kingdom
(Received 19 October 2011; published 24 February 2012)

The resonant-state expansion (RSE), a rigorous perturbation theory of the Brillouin-Wigner type recently developed in electrodynamics [E. A. Muljarov, W. Langbein, and R. Zimmermann, Europhys. Lett. **92**, 50010 (2010)], is applied to planar, effectively one-dimensional optical systems, such as layered dielectric slabs and Bragg reflector microcavities. It is demonstrated that the RSE converges with a power law in the basis size. Algorithms for error estimation and their reduction by extrapolation are presented and evaluated. Complex eigenfrequencies, electromagnetic fields, and the Green's function of a selection of optical systems are calculated, as well as the observable transmission spectra. In particular, we find that for a Bragg-mirror microcavity, which has sharp resonances in the spectrum, the transmission calculated using the RSE reproduces the result of the transfer- or scattering-matrix method.

DOI: 10.1103/PhysRevA.85.023835 PACS number(s): 42.25.−p, 03.50.De, 03.65.Nk

I. INTRODUCTION

Recently, a rigorous perturbation method for the treatment of open electromagnetic systems, the resonant-state expansion (RSE), has been formulated [1]. Unlike previous perturbative approaches [2–7], which due to their complexity and poor convergency are limited to small perturbations, this method is shown to be suitable for perturbations of arbitrary strength and shape. It is based on the concept of resonant states (RSs) of an open system, also known in quantum mechanics as Gamow [8] or Siegert states [9,10]. These states exponentially decay in time and grow in space at large distances [11]. Owing to their completeness inside a finite area of space, RSs can be used for expanding solutions of the Maxwell equations, reducing the wave problem for the modes of the system to diagonalization of a finite complex matrix. Hence the strength and the shape of the perturbed dielectric profile that can be treated is limited only by the size of the chosen finite basis of unperturbed RSs.

The idea of resonances is a cornerstone of physics, allowing one to rationalize the dynamic behavior of physical systems. In open systems, excitations decay with time, endowing resonances with a spectral width. Depending on their width and separation, resonances appear in measured spectra as isolated lines or merge into a continuum. The concept of RSs provides a unified picture of an open system which includes all types of resonances and is an alternative to the commonplace division of the spectrum into nondecaying bound and continuum states with real energies. RSs are discrete eigenstates which have complex frequencies (and equivalently energies and wave numbers) and satisfy outgoing wave boundary conditions. This corresponds to a physical situation where an open system, excited at an earlier time, loses its energy to the outside space. The imaginary part of the frequency reflects the temporal decay of the energy in the system. Owing to this leakage, the RS wave functions have tails (outgoing waves) which grow exponentially outside of the system and cannot be normalized by the usual integration of their square modulus. Instead, the normalization and orthogonality of RSs is given by an integral over the finite volume of the system and the energy flux to the outside in the form of a surface term [9,12].

The presence of a continuum in the spectrum of a system is a significant problem for any perturbation theory. In open electromagnetic systems such a continuum is often the dominating, if not the only, part of the spectrum. However, going away from the real axis to the complex frequency plane, the continuum can in many cases be effectively replaced by a countable number of discrete RSs which form a complete basis. Therefore, RSs of a perturbed system can be expanded into the unperturbed RSs. The expansion coefficients can be found by diagonalizing a complex symmetric matrix which consists of a diagonal matrix representing the bare spectrum, and the perturbation [1]. The perturbed resonant states can then be used to calculate the Green's function of the system via its spectral representation [13,14], using the Mittag-Leffler theorem. The Green's function provides the complete system response and allows one to calculate observables such as emission, scattering, or transmission. This recently formulated general method of reducing the Maxwell equations for an open optical system to a linear matrix eigenvalue problem is called RSE.

The RSE has been suggested [1] as an appropriate tool for calculation of sharp resonances in optical spectra, such as perturbed whispering gallery modes of a dielectric microsphere. Popular computational techniques in electrodynamics, such as the finite difference in time domain (FDTD) [15,16] or the finite element method [17–19] adapted to such problems, require a large computational domain in time and/or space, and can produce spurious solutions [20]. In particular, sharp resonances are characterized by optical modes which decay slowly in time and hence FDTD needs a large time domain. Furthermore, being applied to open systems, the finite element method either introduces a significant error when the boundary is too close, or needs to consider an excessively large domain in real space in order to describe the far-field asymptotics correctly. The RSE does not suffer from these problems because it produces the eigenstates of the system, and in particular their wave numbers, directly by diagonalization of a matrix determined by the near-field properties only.

In this paper, we develop the RSE into a well-defined practical method for calculating RSs as well as transmission and scattering properties of an open optical system, and

*On leave from General Physics Institute RAS, Moscow, Russia; egor.muljarov@astro.cf.ac.uk

we demonstrate its performance on several realistic structures. We provide an efficient algorithm estimating error and extrapolating the RSs, yielding results of improved and defined accuracy. Specifically, we apply the RSE outlined in Sec. II to planar optical systems. For such effectively one-dimensional (1D) systems, efficient alternative methods exist to calculate the transmission and reflection, enabling verification of the RSE results. We investigate the accuracy with which eigenfrequencies, eigenfunctions, the Green's function, and transmission can be reproduced. We give a method to evaluate the convergence and to extrapolate the results in Sec. III. We apply the RSE to a perturbed dielectric slab in Sec. IV with two different kinds of perturbation: a wide-layer perturbation and a δ perturbation. We find that the RSE converges to the exact solution with a power law in the basis size. As an example of a structure with a sharp resonance, we treat a Bragg-mirror microcavity in Sec. IV E.

II. THE PERTURBATION METHOD

The system of Maxwell's equations for a planar dielectric structure with permeability $\mu = 1$ surrounded by vacuum is reduced to the following wave equation:

$$\partial_z^2 \mathbb{E}_\nu(z,t) = c^{-2}[\varepsilon(z) + \Delta\varepsilon(z)]\partial_t^2 \mathbb{E}_\nu(z,t), \tag{1}$$

where $\varepsilon(z)$ denotes the unperturbed dielectric profile, and $\Delta\varepsilon(z)$ the perturbation of the dielectric function. Here the transverse eigenmodes with index ν are taken with zero in-plane wave number. The electric field $\mathbb{E}_\nu(z,t)$ can be written in a harmonic form

$$\mathbb{E}_\nu(z,t) = \mathcal{E}_\nu(z)\exp(-ic\varkappa_\nu t), \tag{2}$$

with complex frequency $c\varkappa_\nu$ (c is the speed of light in vacuum) and amplitude $\mathcal{E}_\nu(z)$ satisfying the following time-independent wave equation:

$$\left\{\partial_z^2 + [\varepsilon(z) + \Delta\varepsilon(z)]\varkappa_\nu^2\right\}\mathcal{E}_\nu(z) = 0. \tag{3}$$

The electric field $\mathcal{E}_\nu(z)$ and its first derivative are continuous everywhere. RSs are eigenmodes which satisfy outgoing boundary conditions, given by the form

$$\mathcal{E}_\nu(z) = A_\nu^{\pm}\ \exp(i\varkappa_\nu|z|) \tag{4}$$

in the surrounding vacuum with the amplitudes A_ν^- (on the left-hand side) and A_ν^+ (on the right-hand side of the structure) which are generally different. In the case of a mirror-symmetric system, $A_\nu^- = A_\nu^+$ for symmetric and $A_\nu^- = -A_\nu^+$ for antisymmetric modes.

In the following, for the unperturbed RSs, i.e., for $\Delta\varepsilon(z) = 0$, $\mathcal{E}_\nu(z)$ is denoted as $E_n(z)$, and $\varkappa_\nu$ as k_n. The unperturbed RSs are orthogonal and normalized according to

$$\int_{-a}^{a} \varepsilon(z)E_n(z)E_m(z)dz - \frac{E_n(-a)E_m(-a) + E_n(a)E_m(a)}{i(k_n + k_m)} = \delta_{nm}, \tag{5}$$

where $z = \pm a$ are the positions of the boundaries of the unperturbed system. The perturbed states are written as linear combinations of the normalized unperturbed RSs,

$$\mathcal{E}_\nu(z) = \sum_n c_{n\nu}\frac{E_n(z)}{\sqrt{k_n}}, \tag{6}$$

resulting in the linear eigenvalue problem for $\varkappa_\nu$ and $c_{n\nu}$,

$$\sum_m \left(\frac{\delta_{nm}}{k_n} + \frac{V_{nm}}{2\sqrt{k_n k_m}}\right)c_{m\nu} = \frac{1}{\varkappa_\nu}c_{n\nu}, \tag{7}$$

with the perturbation matrix [1]

$$V_{nm} = \int_{-a}^{a} \Delta\varepsilon(z)E_n(z)E_m(z)\,dz. \tag{8}$$

In a dielectric system with real refractive index, the RSs have the following general property: Im $k_n \leqslant 0$ and $k_{-n} = -k_{+n}^*$ along with $E_{-n} = E_n^*$. Additionally, in 1D systems (planar systems at normal incidence) there is always a RS with Re $k_0 = 0$ and Im $k_0 < 0$. We number the RSs with increasing real part of their wave number, numbering the state with zero real part as state number zero. The number of RSs in the unperturbed or perturbed systems is countably infinite. Therefore we always deal with a truncation of the basis of the RS, which is the only approximation of the theory. We refer to $n_{\max}$ as the truncation number for the basis so that $-n_{\max} \leqslant n \leqslant n_{\max}$. Hence the basis size N is given by

$$N = 2n_{\max} + 1. \tag{9}$$

Ideally, by choosing the basis size N sufficiently large, the results of the perturbation theory can be produced with any given accuracy. An earlier perturbative approach of Brillouin-Wigner type [21] treating a one-dimensional half-space yielded a nonlinear matrix eigenvalue problem and was not further developed.

The unperturbed system can be any convenient system. In the discussed 1D case, a dielectric slab in vacuum having thickness $2a$ and real dielectric constant

$$\varepsilon(z) = \begin{cases} \epsilon_s & \text{for} \quad |z| < a \\ 1 & \text{otherwise} \end{cases} \tag{10}$$

is the simplest system having an analytic solution. We use it as an unperturbed system in the following. The expressions for the unperturbed RSs given in the Appendix. The dielectric constant is taken to be $\sqrt{\epsilon_s} = 1.5$ unless otherwise stated.

III. CONVERGENCE AND EXTRAPOLATION

As we increase the size N of the basis, a given perturbed RS eventually converges to the exact solution. It was noted earlier [1] for specific examples that this convergence was following an N^{-3} scaling. We found that in general the convergence is following a power law in the basis size, which allows us to estimate the remaining error for finite basis sizes. Furthermore, we provide an extrapolation algorithm using this scaling which significantly improves the accuracy of the RS.

We consider the RS wave numbers calculated via the perturbation theory $\varkappa_\nu^{(N)}$ and their exact values $\varkappa_\nu^{(\text{exact})}$ and

suppose that the absolute error in each wave number scales as a power law in the basis size N:

$$\varkappa_\nu^{(\mathrm{exact})} - \varkappa_\nu^{(N)} \approx K_\nu N^{\alpha_\nu}. \tag{11}$$

We assume that the exponent in the power law (α_ν) is a real number, so that the RS wave numbers converge in a straight line in the complex plane. To determine K_ν, α_ν, and $\varkappa_\nu^{(\mathrm{exact})}$ in Eq. (11) from the RSE, we need $\varkappa_\nu^{(N)}$ for a triplet of different N. In order to estimate the error of the extrapolation, we use two triplets, namely, $\{N_1,N_2,N_4\}$ yielding K'_ν,α'_ν, and $\{N_2,N_3,N_4\}$ yielding K''_ν,α''_ν. We choose the sizes as

$$N_1 \approx \eta^4 N_4, \quad N_2 \approx \eta^2 N_4, \quad N_3 \approx \eta N_4, \tag{12}$$

with the factor $0 < \eta < 1$, yielding analytic expressions shown later.

For each size we calculate the set of RSs with the RSE. We match the RSs between the four sets sequentially, i.e., first $\{\varkappa_\nu^{(N_4)}\}$ to $\{\varkappa_\nu^{(N_3)}\}$, then $\{\varkappa_\nu^{(N_3)}\}$ to $\{\varkappa_\nu^{(N_2)}\}$, and finally $\{\varkappa_\nu^{(N_2)}\}$ to $\{\varkappa_\nu^{(N_1)}\}$. In doing this, we use the following matching algorithm (MA) between two sets of wave numbers, $\{\varkappa_\nu^{(\mathrm{A})}\}$ and $\{\varkappa_\nu^{(\mathrm{B})}\}$:

(a) Determine the distance between the complex wave numbers of all pairs with one element from $\{\varkappa_\nu^{(\mathrm{A})}\}$ and one element from $\{\varkappa_\nu^{(\mathrm{B})}\}$.

(b) Select the pair with the shortest distance, store it, and remove it from the sets.

(c) Repeat (b) until $\{\varkappa_\nu^{(\mathrm{A})}\}$ or $\{\varkappa_\nu^{(\mathrm{B})}\}$ is empty.

This procedure results in N_1 vectors $(\varkappa_\nu^{(N_1)},\varkappa_\nu^{(N_2)},\varkappa_\nu^{(N_3)},\varkappa_\nu^{(N_4)})$ of RS wave numbers. The specific factors chosen between N_1, N_2, N_3, and N_4 allow for the following analytical expressions for two sets of coefficients and exponents in Eq. (11), for each state ν:

$$\alpha'_\nu = \frac{1}{2\ln\eta}\ln\left(\left|\frac{\varkappa_\nu^{(N_4)} - \varkappa_\nu^{(N_1)}}{\varkappa_\nu^{(N_4)} - \varkappa_\nu^{(N_2)}}\right| - 1\right), \tag{13}$$

$$\alpha''_\nu = \frac{1}{\ln\eta}\ln\left(\left|\frac{\varkappa_\nu^{(N_4)} - \varkappa_\nu^{(N_2)}}{\varkappa_\nu^{(N_4)} - \varkappa_\nu^{(N_3)}}\right| - 1\right), \tag{14}$$

$$K'_\nu = \frac{\varkappa_\nu^{(N_4)} - \varkappa_\nu^{(N_2)}}{N_2^{\alpha'_\nu} - N_4^{\alpha'_\nu}}, \tag{15}$$

$$K''_\nu = \frac{\varkappa_\nu^{(N_4)} - \varkappa_\nu^{(N_3)}}{N_3^{\alpha''_\nu} - N_4^{\alpha''_\nu}}. \tag{16}$$

For extrapolation of eigenvalues and estimation of errors we use the mean values

$$\alpha_\nu = \frac{\alpha'_\nu + \alpha''_\nu}{2}, \quad K_\nu N_4^{\alpha_\nu} = \frac{K'_\nu N_4^{\alpha'_\nu} + K''_\nu N_4^{\alpha''_\nu}}{2}. \tag{17}$$

In order to test the quality of our power-law fit, we estimate for each state ν the relative extrapolation error defined as

$$F_\nu = \Phi\left(K'_\nu N_4^{\alpha'_\nu}, K''_\nu N_4^{\alpha''_\nu}\right), \tag{18}$$

where $2\Phi(X,Y) = \Gamma(X,Y) + \Gamma(Y,X)$ and

$$\Gamma(X,Y) = \left|\frac{X}{Y} - 1\right|. \tag{19}$$

Indeed, F_ν has the meaning of a relative error in the power-law approximation of the distance $\varkappa_\nu^{(\mathrm{exact})} - \varkappa_\nu^{(N_4)}$ deduced from the two sets of power-law parameters. If this error is sufficiently small, $F_\nu < F_{\max}$, and the power law converges sufficiently fast ($\alpha_\nu < \alpha_{\max}$), we can improve the result calculated for the largest basis size N_4 by extrapolating it toward the exact value, $\varkappa_\nu^{(N_4)} \to \varkappa_\nu^{(\infty)}$, where the extrapolated wave vector $\varkappa_\nu^{(\infty)}$ is defined according to Eq. (11) as

$$\varkappa_\nu^{(\infty)} = \varkappa_\nu^{(N_4)} + K_\nu N_4^{\alpha_\nu}. \tag{20}$$

Otherwise, the power law is not describing the convergence well. We then use the absolute variation scaled to the system size to evaluate if the state has sufficiently converged

$$M_\nu = \max_{i=1,2,3}\left|\varkappa_\nu^{(N_4)} - \varkappa_\nu^{(N_i)}\right| a. \tag{21}$$

We use state ν for the calculation of the Green's function and/or transmission if its relative or absolute error is sufficiently small, i.e., if one of the two selection criteria (SC) is met: (1) extrapolation error $F_\nu|K_\nu N_4^{\alpha_\nu}|a < M_{\max}$, provided that $F_\nu < F_{\max}$ and $\alpha_\nu < \alpha_{\max}$ or, (2) absolute error $M_\nu < M_{\max}$. For the results shown in the present paper we used $M_{\max} = 0.1$, $F_{\max} = 1$, $\alpha_{\max} = -0.5$, and $\eta = 2^{-1/4}$.

We can estimate the resulting numerical complexity of this method as follows. For a sufficiently large basis size N, the numerical complexity calculating the RS wave numbers is governed by the time required for diagonalization of an $N \times N$ complex matrix [see Eq. (7)] scaling as N^3. To produce the four sets of RSs used above, the complexity is $(1+\eta^3+\eta^6+\eta^{12})N_4^3 \approx 2N_4^3$. For reference, the diagonalization time for $N = 10^3$ is in the order of seconds on a modern PC.

IV. RESULTS

A. Wide-layer perturbation

The perturbation being considered in this section is given by

$$\Delta\varepsilon(z) = \begin{cases} \Delta\epsilon & \text{for } a/2 \leqslant z \leqslant a \\ 0 & \text{otherwise,} \end{cases} \tag{22}$$

with $\Delta\epsilon = 10$. The profiles of the unperturbed and perturbed dielectric constants are shown in Fig. 1. The analytic solutions of the time-independent Maxwell equations using the RS boundary conditions are given in the Appendix, both for the unperturbed and the perturbed systems, along with the matrix elements V_{nm} of the perturbation.

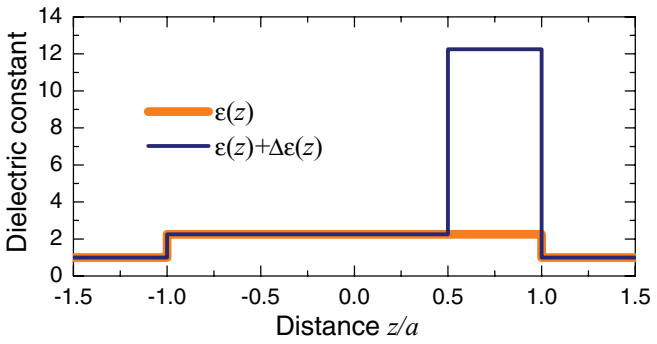

FIG. 1. (Color online) Dielectric constants of the unperturbed slab $\varepsilon(z)$ and a slab with a wide perturbation $\varepsilon(z) + \Delta\varepsilon(z)$. The distance z is in units of the half width a of the slab.

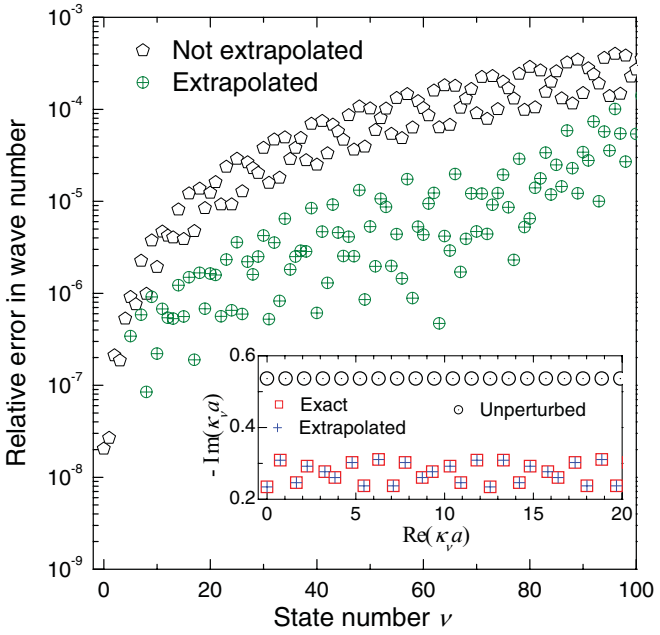

FIG. 2. (Color online) Relative errors $\Gamma(\varkappa_\nu^{(\infty)}, \varkappa_\nu^{(\text{exact})})$ and $\Gamma(\varkappa_\nu^{(N_4)}, \varkappa_\nu^{(\text{exact})})$ of the RS wave vectors calculated via the RSE for the perturbation shown in Fig. 1, with and without extrapolation, respectively, for $N_4 = 801$. Inset: unperturbed and perturbed RS wave numbers; the latter are calculated analytically (empty squares) and via the RSE with extrapolation (crosses).

Using the procedure introduced in Sec. III we calculate four sets of perturbed wave numbers and extrapolate $\varkappa_\nu$ according to Eq. (20). We also calculate the exact wave numbers $\varkappa_\nu^{(\text{exact})}$ and match up exact and perturbed states using the MA. The resulting exact and extrapolated eigenvalues $\varkappa_\nu^{(\infty)}$ are shown in the inset of Fig. 2, together with the unperturbed wave vectors. We measure the errors in $\varkappa_\nu^{(\infty)}$ relative to $\varkappa_\nu^{(\text{exact})}$ by $\Gamma(\varkappa_\nu^{(\infty)}, \varkappa_\nu^{(\text{exact})})$ and compare it with $\Gamma(\varkappa_\nu^{(N_4)}, \varkappa_\nu^{(\text{exact})})$ to evaluate the extrapolation method. The results are shown in Fig. 2. We see that the relative error of the RS wave number is generally reduced by extrapolation by more than one order of magnitude.

The coefficients and exponents of the power-law fit give us information about the convergence properties of the perturbed RSs. For the wide perturbed layer they are shown in Fig. 3. We see in Fig. 3(a) that states close to the origin in complex wave number space (and having small state number values) are not described well by the power law (F_ν is larger than $F_{\max}$), even though Fig. 2 suggests that these states are well converged. This is reflected in the small absolute error M_ν shown in Figs. 3(g) and 3(h), passing the SC. We also see that for higher wave-number states passing the relative SC the exponent in the power law is close to $\alpha = -3$ [horizontal lines in Figs. 3(c) and 3(d)], in accordance with the findings in Ref. [1].

Furthermore, the absolute errors $K_\nu N^{\alpha_\nu}$ and M_ν show universal dependencies on the normalized state number $\nu/n_{\max}$, as shown in Figs. 3(f) and 3(h). This provides us with a scaling law of the absolute errors versus the state number:

$$M_\nu \propto (\nu/N)^3. \tag{23}$$

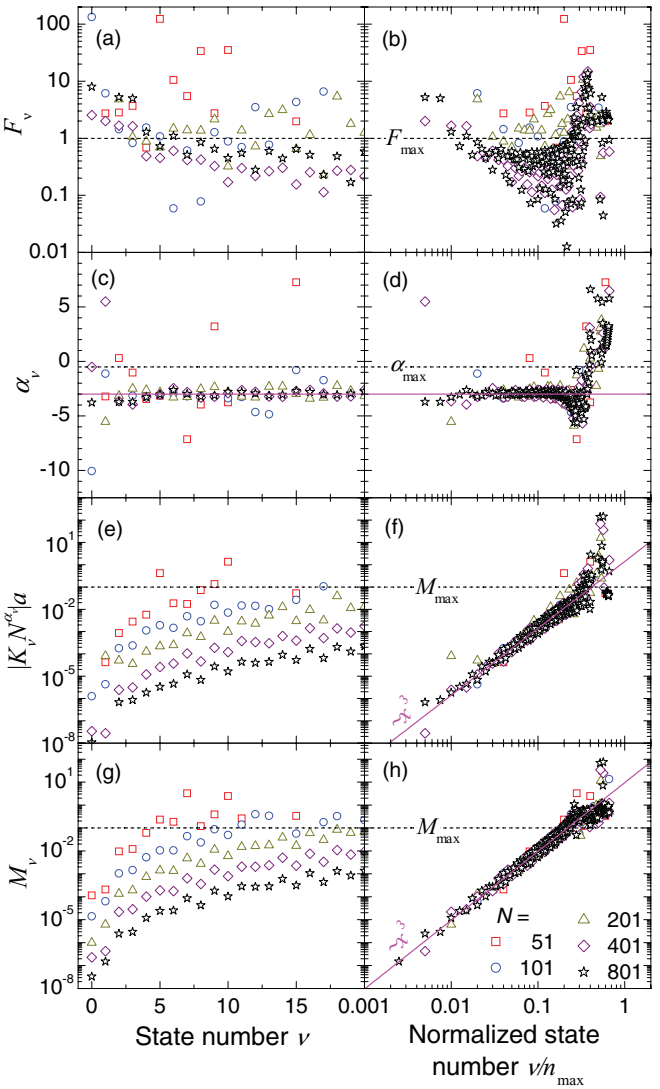

FIG. 3. (Color online) Power law parameters and error estimates for the wide perturbation. [(a),(b)]: Relative extrapolation error F_ν, [(c),(d)]: exponent α_ν in the power law fit, [(e),(f)]: absolute errors $K_\nu N_4^{\alpha\nu}$, and [(g),(h)] M_ν as functions of the state number ν, calculated for different basis size N. The right panels display the data versus the state number ν normalized to its maximum value $n_{\max} = (N-1)/2$. Straight magenta lines are $\alpha = -3$ [(c),(d)] and power law fits [(h),(f)].

This cubic scaling is shown in Figs. 3(f) and 3(h) by straight magenta lines. The power-law exponent α also shows a universal dependency on the normalized state number, being $\alpha = -3$ for $\nu/n_{\max} \lesssim 0.2$ as can be seen in Fig. 3(d). In this region the states pass the relative SC and are extrapolated.

An example of how the power law is applied to extrapolate the wave number of a particular state $\nu = 63$ is given in Fig. 4(a). Clearly, the extrapolation leads to a considerable improvement of the accuracy compared to the wave number calculated with the maximum matrix size N_4. This is due to the good power-law convergence as shown in Fig. 4(b), seen by the straight line connecting the "exact" errors $|\varkappa_\nu^{(\text{exact})} - \varkappa_\nu^{(N_i)}|$ for the four basis sizes.

The exact errors are only available if the exact solution is known, but in this ideal case we do not need the RSE. In a

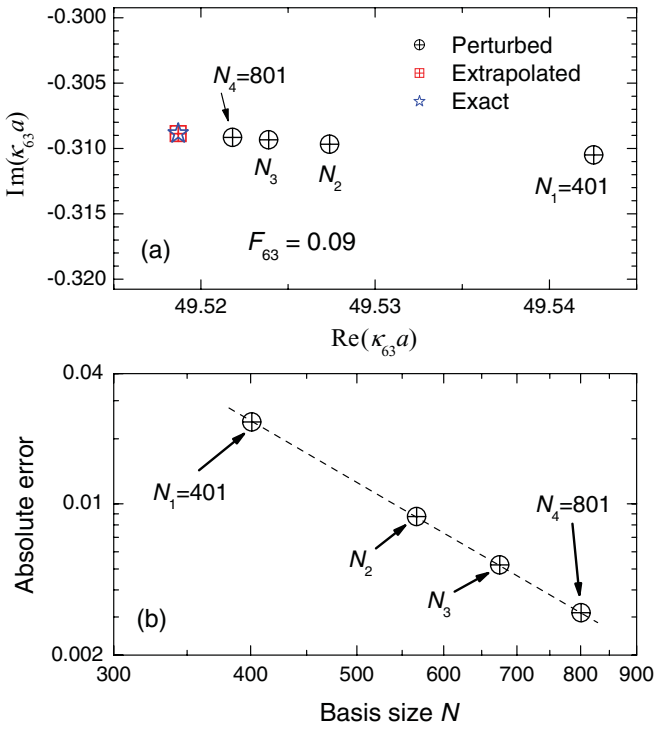

FIG. 4. (Color online) (a) Wave number of the perturbed state $\nu = 63$ calculated with different basis size N and extrapolated to the exact value. (b) Absolute "exact" error $|\varkappa_{63}^{(\mathrm{exact})} - \varkappa_{63}^{(N)}|$ for different N (squares) and a power-law fit (dashed line).

realistic case for which no such solution is known, we need to estimate the error of the power-law extrapolation, which we do using the extrapolation SC and Eq. (18). In order to check how good this estimation is, we compare F_ν with the exact relative extrapolation error $F_\nu^{(\mathrm{exact})} = \Phi(K_\nu N_4^{\alpha_\nu}, \varkappa_\nu^{(\mathrm{exact})} - \varkappa_\nu^{(N_4)})$. Such a comparison is shown in Fig. 5 for all states with $\alpha_\nu < -0.5$. We can see that the exact error $F_\nu^{(\mathrm{exact})}$ is typically overestimated by F_ν, and for all states with $F_\nu < F_{\max}$ we have $F_\nu^{(\mathrm{exact})} < 1$, i.e., the extrapolation is improving the error. F_ν can thus be used reliably to verify the convergency and power-law extrapolation.

B. Electric fields

The electric fields (EFs) $\mathcal{E}_\nu(z)$ of the perturbed RSs calculated via the exact formula (A5) are shown in Fig. 6 for a few lowest states in comparison with $E_n(z)$, the EFs of the unperturbed RSs, given by Eq. (A1). The perturbed RSs are normalized as in Eq. (5). In particular, their orthonormality condition reads

$$\int_{-a}^{a} \varepsilon_p(z)\mathcal{E}_\nu(z)\mathcal{E}_\mu(z)dz - \frac{\mathcal{E}_\nu(-a)\mathcal{E}_\mu(-a) + \mathcal{E}_\nu(a)\mathcal{E}_\mu(a)}{i(\varkappa_\nu + \varkappa_\mu)} = \delta_{\nu\mu}, \qquad (24)$$

where $\varepsilon_p(z) = \varepsilon(z) + \Delta\varepsilon(z)$ is the perturbed dielectric profile. All unperturbed states have the same imaginary part of their wave vectors (see the inset of Fig. 2) and thus their fields have all the same envelope, exponentially growing outside the slab, with the higher-n states oscillating more rapidly [see Fig. 6(a)].

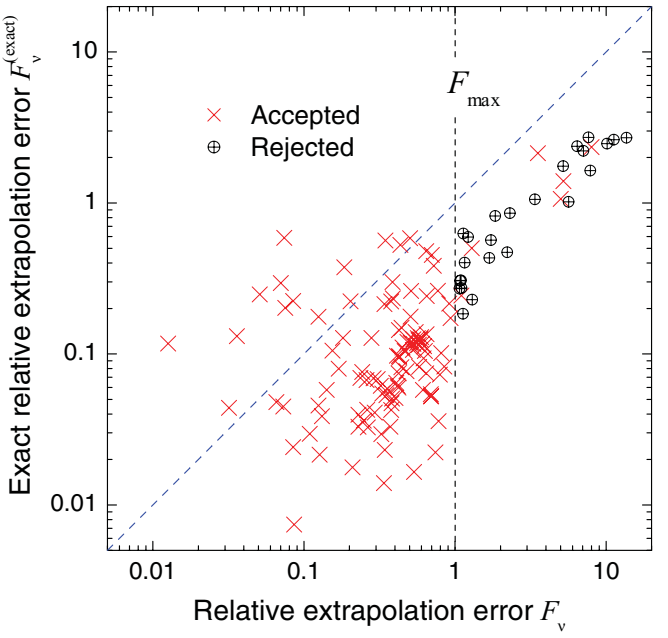

FIG. 5. (Color online) Exact relative extrapolation error $F_\nu^{(\mathrm{exact})}$ versus relative extrapolation error F_ν for both accepted and rejected states, for $N_4 = 801$. The blue dashed line shows the anticipated behavior $F_\nu^{(\mathrm{exact})} \approx F_\nu$.

In the perturbed system, the envelopes are different due the varying Im $\varkappa_\nu$. Also, as can be seen in Fig. 6(b), the frequency of the oscillations increases in the perturbed (denser) layer, and their amplitudes change at the same time.

The perturbation theory fully reproduces the EFs of the RSs, both inside and outside the slab. Inside the slab, the EF is given by the expansion in Eq. (6) with the coefficients $c_{n\nu}$ diagonalizing the matrix in Eq. (7). Outside the slab, the fields

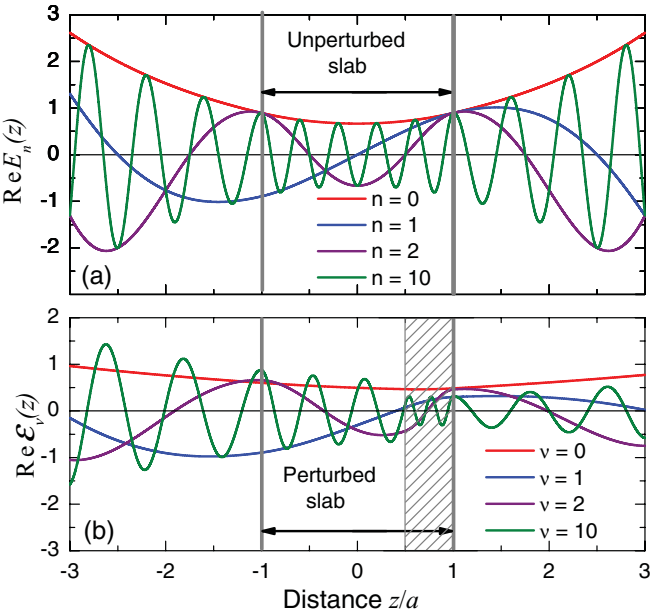

FIG. 6. (Color online) Real part of the normalized electric field of a few lowest-energy RSs of the unperturbed slab (a) and of the perturbed slab (b).

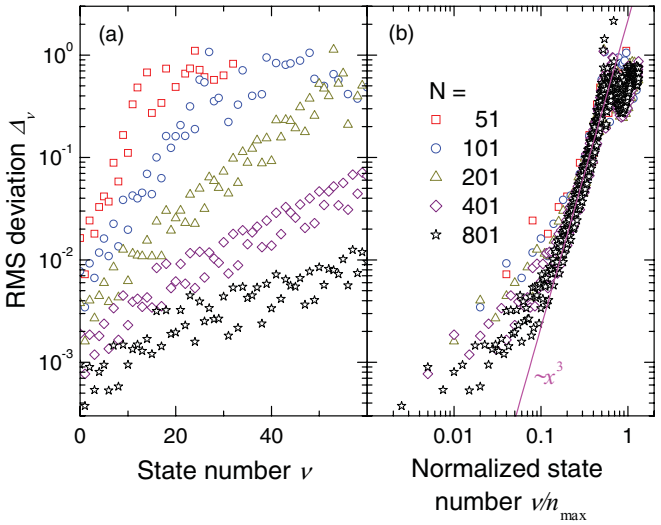

FIG. 7. (Color online) Root-mean-square deviation of the RS electric field $\mathcal{E}_\nu^N$ from its exact value $\mathcal{E}_\nu^{(\text{exact})}$ versus the state number ν (a) and normalized state number $\nu/n_{\max}$ (b), calculated for different basis size N. The straight magenta line in (b) is a cubic law fit.

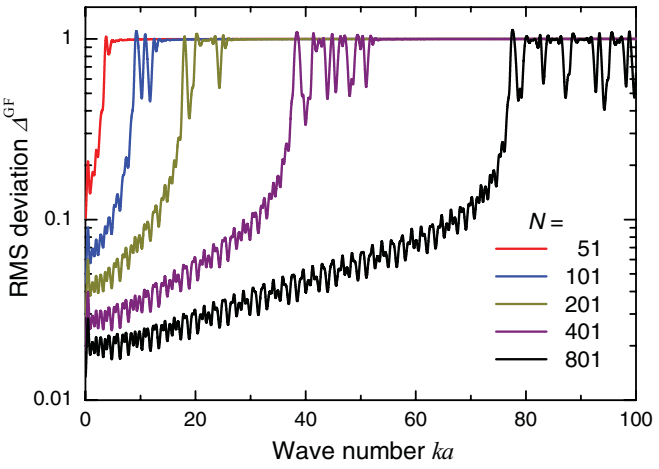

FIG. 8. (Color online) The root-mean-square deviation in the GF Δ^{GF} as a function of the wave number of the driving field k, calculated via the RSE for different basis size N.

are given by Eq. (4) in which the perturbed wave vectors $\varkappa_\nu$ assign the proper exponential growth and oscillations of the EF in vacuum, while the amplitudes $A_\nu^\pm$ are found by comparing Eqs. (4) and (6) and using the continuity of the EF through the boundaries. To quantify how well the perturbation theory reproduces the EF of a RS, we calculate its root-mean-square (RMS) deviation within the system defined by

$$\Delta_\nu = \sqrt{\frac{\int_{-a}^{a} \left|\mathcal{E}_\nu^{(N)}(z) - \mathcal{E}_\nu^{(\text{exact})}(z)\right|^2 dz}{\int_{-a}^{a} \left|\mathcal{E}_\nu^{(\text{exact})}(z)\right|^2 dz}}. \tag{25}$$

The results are shown in Fig. 7, where we have matched exact and perturbed RSs using the MA and plotted Δ_ν for different basis size N. We see that the trend in accuracy with state number and the basis size is the same as in Figs. 3(e) and 3(g), and the rms deviation versus the normalized state number also shows a universal dependence similar to those in Figs. 3(f) and 3(h). However, the EF is, in general, less well reproduced than the wave numbers, and the power law $\Delta_\nu \propto (\nu/N)^3$ is observed only in the interval of $0.05 < \Delta_\nu < 0.2$.

C. Green's function and transmission

The Green's function (GF) is an important quantity which fully characterizes the response of an optical system, determining its scattering and transmission. For the slab with a wide perturbed layer given by Eqs. (10) and (22), the GF $G(z,z';k)$ which satisfies the equation

$$\left\{\partial_z^2 + [\varepsilon(z) + \Delta\varepsilon(z)]k^2\right\} G(z,z';k) = \delta(z - z') \tag{26}$$

and outgoing boundary conditions can be calculated analytically. Note that when calculating observables, k is real as it is given by the vacuum wave number of an external driving field. The GF is calculated using its spectral representation [1,13,14],

$$G(z,z';k) = \sum_\nu \frac{\mathcal{E}_\nu(z)\mathcal{E}_\nu(z')}{2k(k - \varkappa_\nu)}, \tag{27}$$

in which the EF $\mathcal{E}_\nu(z)$ and the RS wave numbers $\varkappa_\nu$ are calculated numerically via the RSE. For the wave numbers $\varkappa_\nu$, we use the extrapolated values, Eq. (20).

In light of the importance of the GF and its further usage for calculation of observables, we compare $G^{(N)}$, the GF calculated by RSE with basis size N and Eq. (27), to its exact analytic form $G^{(\text{exact})}$, again using the RMS deviation as given by

$$\Delta^{\text{GF}} = \sqrt{\frac{\int_{-a}^{a}\int_{-a}^{a} |G^{(N)}(z,z') - G^{(\text{exact})}(z,z')|^2 \, dz\, dz'}{\int_{-a}^{a}\int_{-a}^{a} |G^{(\text{exact})}(z,z')|^2 \, dz\, dz'}}. \tag{28}$$

Such a comparison is shown in Fig. 8 for different basis size N. Increasing the basis size has two effects on the GF: (i) it improves the GF error at a given k and (ii) widens the k range of the GF with small error. The latter is due to a larger wave-number range of poles in the GF [Eq. (27)], being reproduced for large N.

Both expansions [Eqs. (6) and (27)], for the EF and for the GF, are valid only inside the slab or on its borders and are not suitable for the vacuum area where the EFs of the RSs grow exponentially. The GF itself is, however, regular on the real k axis and does not grow exponentially. Moreover, in vacuum, it always has a simple analytic form of a plane wave with the amplitude that can be deduced from values inside the slab [Eq. (27)], using the continuity of the GF when passing through the interfaces. In this way, the GF can be calculated at any point of the (z,z') space, inside or outside the slab.

The delta function in Eq. (26) plays the role of a source of plane waves generated at the point z' and propagating in both directions, away from the source. The GF then has the meaning of the system's response to such a plane-wave excitation. This can be used to derive a formula for the transmission in terms of the GF. To do this, we place the source of strength $2ik$ just outside the slab at $z' = -a$, in order to produce two plane waves of amplitude 1. One of these waves is transmitted trough the slab, and just after the slab at point $z = a$ the intensity of

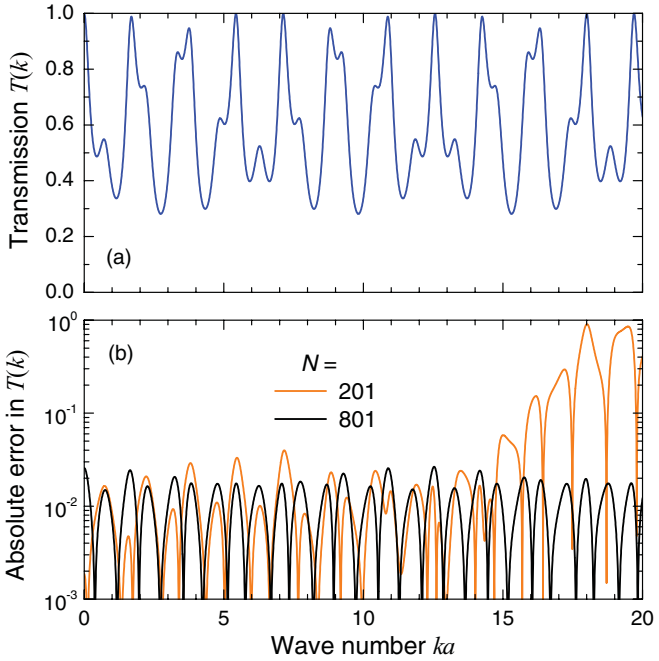

FIG. 9. (Color online) (a) Light transmission through the slab with a wide-layer perturbation, Eq. (22). (b) Absolute error in the transmission calculated using the analytic form of $T(k)$ and numerical values from the RSE for two different simulations.

the EF (which does not change with further increase of z) is given by

$$T(k) = |2kG(a, -a; k)|^2 \tag{29}$$

and is called transmission.

We calculate the transmission using Eq. (29) for the GF taken to be either numerical $G^{(N)}$ or analytical $G^{(\text{exact})}$. This allows us to calculate the absolute error in the transmission, $|T^{(N)} - T^{(\text{exact})}|$, which is shown in Fig. 9(b). The transmission itself is shown in Fig. 9(a) and has a profile which is fully determined by the pole structure of the GF. The RSs which contribute in this frequency range can be seen in the inset of Fig. 2. We see that the error of the transmission has a similar magnitude and scaling with N as the GF itself, as can be expected from Eq. (29).

D. δ perturbation

We now move from a wide perturbation to a very narrow and strong one, such as a thin metal film on a dielectric. Such a perturbation is described by

$$\Delta\varepsilon(z) = w\epsilon_d \delta(z - a/2), \tag{30}$$

with the delta-scatter strength $w\epsilon_d = -0.1a$. Physically, this perturbation corresponds to a thin layer of the dielectric constant changed by ϵ_d, which is placed at $z = a/2$ and has a width w much narrower than the shortest wavelength of the resonant modes used in the basis. The dielectric profile for the system with the δ perturbation is shown in Fig. 10.

As in the case of a wide-layer perturbation considered in Sec. IV A we plot and compare in Figs. 11–14 the RS wave numbers, calculated exactly and via the RSE with and without

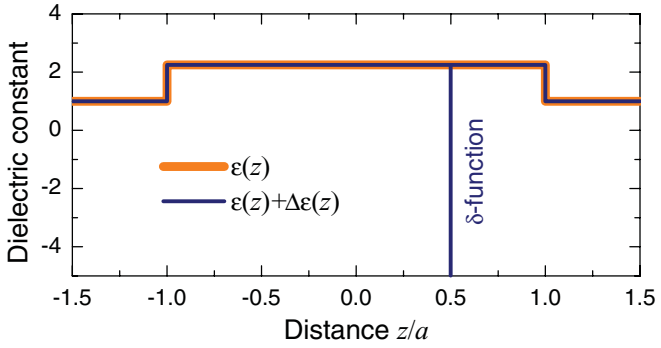

FIG. 10. (Color online) Dielectric constants of the unperturbed slab $\varepsilon(z)$ and a slab with a δ perturbation $\varepsilon(z) + \Delta\varepsilon(z)$. The distance z is in units of the half width a of the slab.

extrapolation, as well as the parameters of the power-law fit and relative and absolute errors which we also need for the quality check of our simulation and extrapolation. The analytic solutions for the δ perturbation and its matrix elements are given in the Appendix.

We see in Fig. 11 that the extrapolation reduces the relative error by one to two orders of magnitude. The integral strength of the perturbation is much (almost two orders of magnitude) weaker than in the case of the wide layer considered in Sec. IV A. However, the convergence is much slower in the case of the δ perturbation. We see in Figs. 12(c) and 12(d) that for large N the power-law exponent is close to $\alpha_\nu = -1$. This is to be expected as the δ perturbation does not have a finite width. The matrix elements V_{nm}, though oscillating, have no decrease with increasing wave number (or index n) which leads to a much stronger mixing of states compared to the wide-layer perturbation. Indeed, in the wide-layer case, states with higher indices are less important due to the rapid oscillation of their wave functions, so that the matrix elements scale as $V_{nm} \propto 1/n$

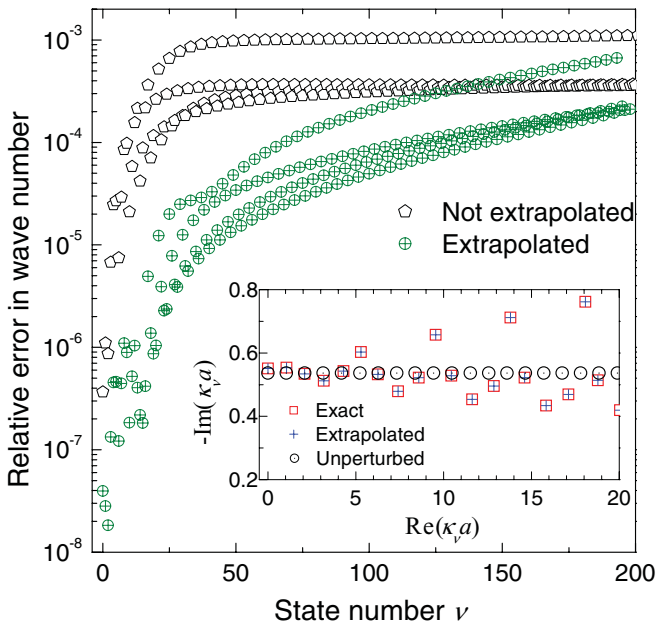

FIG. 11. (Color online) Same as Fig. 2 but for the δ perturbation shown in Fig. 10.

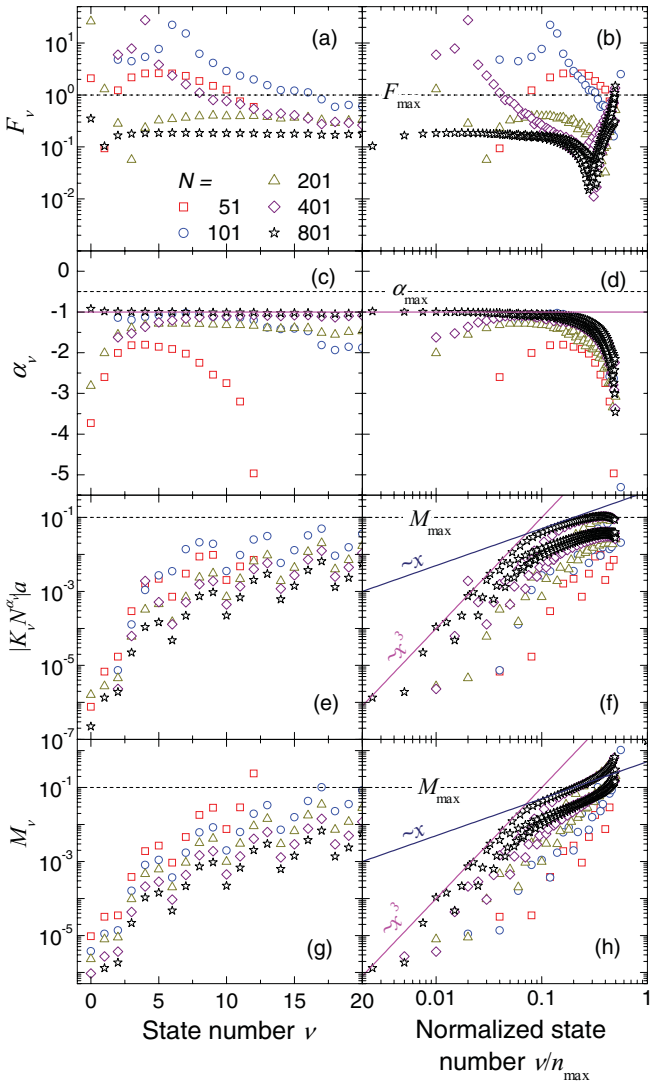

FIG. 12. (Color online) Same as Fig. 3 but for the δ perturbation shown in Fig. 10. The horizontal magenta lines in panels (c) and (d) are $\alpha = -1$ lines.

(for $n \gg m$). Using the second-order Rayleigh-Schrödinger perturbation theory and the explicit form Eqs. (A9) and (A12) of the matrix elements V_{nm}, we can show that the wave-number corrections scale as $1/N$ and $1/N^3$ for the δ- and wide-layer perturbations, respectively, in accordance with Figs. 3(d) and 12(d).

In the case of the δ perturbation, the absolute errors shown in Figs. 12(f) and 12(h) as functions of the normalized state number do not display any universal curves, still, for small ν/N approaching asymptotically a cubic law in the state number ν (magenta lines). Thus we conclude that in this case $M_\nu \propto \nu^3/N$ [compare with Eq. (23)]. At larger values of ν/N this dependence transforms into a linear one, $M_\nu \propto \nu/N$ (blue lines). Because of the slow $(1/N)$ convergence, the extrapolation gives a huge improvement as is clear from Fig. 13 and demonstrates its necessity in the particular case of the δ perturbation.

At the same time, the relative extrapolation error is predicted within an order of magnitude, as can be seen in Fig. 14.

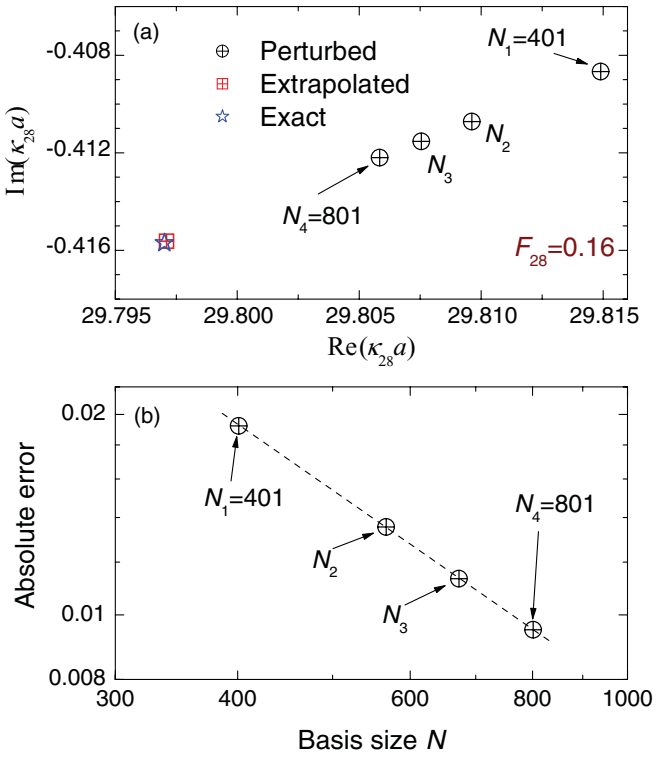

FIG. 13. (Color online) Same as Fig. 4 but for the δ perturbation shown in Fig. 10 and state number $\nu = 28$.

For the majority of RSs, $F_\nu^{(\text{exact})} < F_\nu$, with the exact values $F_\nu^{(\text{exact})}$ being significantly overestimated. However, for a large class of solutions it turns out to be highly underestimated. The systematic deviation seen in Fig. 14 in estimating the relative extrapolation error through F_ν may be a result of the systematic variation in the power-law exponent α_ν well seen in Figs. 12(c) and 12(d). Hence it is generally advisable when studying convergence with our method to run simulations with a variety of N_4 parameters in order to establish over what range of N_4 the power law is applicable for the given strength of perturbation.

We were also able to simulate a δ perturbation outside the perturbed slab by taking the unperturbed slab to include the position of the delta scatterer and thus the perturbation consisting of a superposition of a δ perturbation and a wide layer compensating the difference in the dielectric constants between the vacuum and the unperturbed slab. In this case we did obtain convergence of the perturbed wave numbers to the exact solution. However, for a δ perturbation outside of the unperturbed slab or exactly on the border, the simulation does not converge to the correct solution. This is to be expected since in this case the perturbed RSs contain waves reflected from the external perturbation, which are waves propagating toward the slab. Such incoming waves are not part of the basis of unperturbed RSs, and thus cannot be reproduced by an expansion in this basis.

E. Microcavity

To evaluate the RSE in the presence of sharp resonances, we use a Bragg-mirror microcavity (MC), which consists of a Fabry-Perot cavity of thickness L_C and refractive index n_C

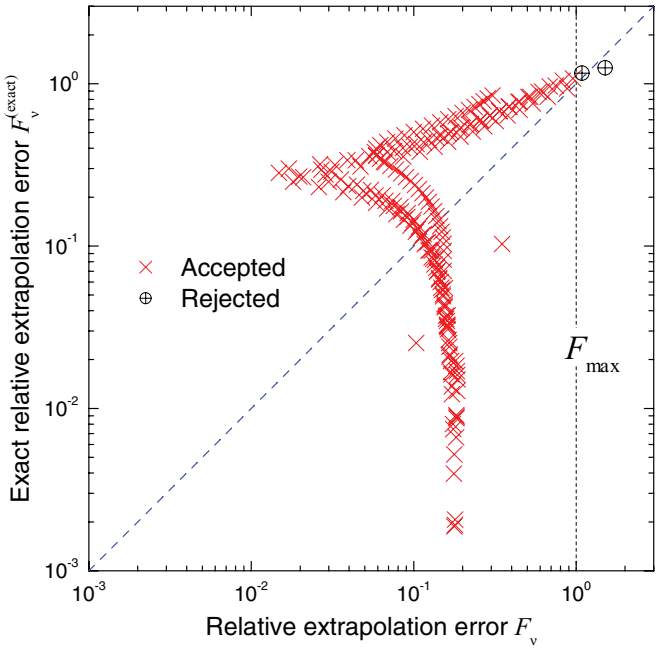

FIG. 14. (Color online) Same as Fig. 5 but for the δ perturbation shown in Fig. 10.

surrounded by distributed Bragg reflectors (DBRs). The DBRs consist of P pairs of dielectric layers with alternating high ($n_H = 3.0$) and low ($n_L = 1.5$) refractive index. In order to have a sharp cavity mode at a given wavelength λ_C, these alternating layers have to be of quarter-wavelength optical thickness, and the optical thickness of the cavity has to be a multiple of half the wavelength. We take $L_C = \lambda_C/2$. An example of the dielectric profile of such a system with $P = 3$ is shown in Fig. 15.

The RSs of a MC are calculated using the RSE. The RS wave vectors and the transmission through the MC are shown in Figs. 16(a) and 16(b). For reference, the unperturbed eigenvalues are also included in Fig. 16(a). The unperturbed system taken for the RSE is again a dielectric slab where dielectric constant $\varepsilon(z)$ can be seen in Fig. 15. Throughout this section the outer boundaries of the MC and the unperturbed slab coincide, and we choose $\epsilon_s = 5.5$ which is between n_L^2 and n_H^2, providing good convergence. ϵ_s could be further

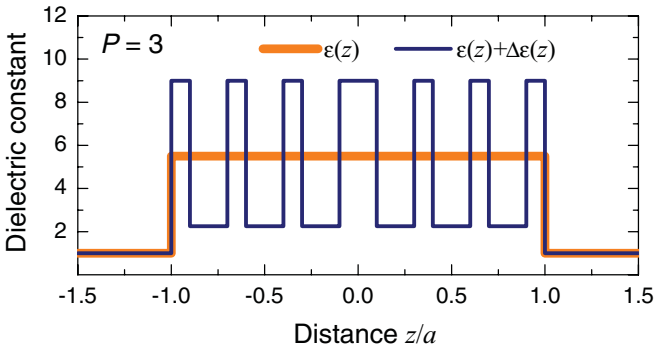

FIG. 15. (Color online) Dielectric profiles of a planar microcavity having $P = 3$ pairs of Bragg mirrors on each side (blue line) and an unperturbed dielectric slab (orange line).

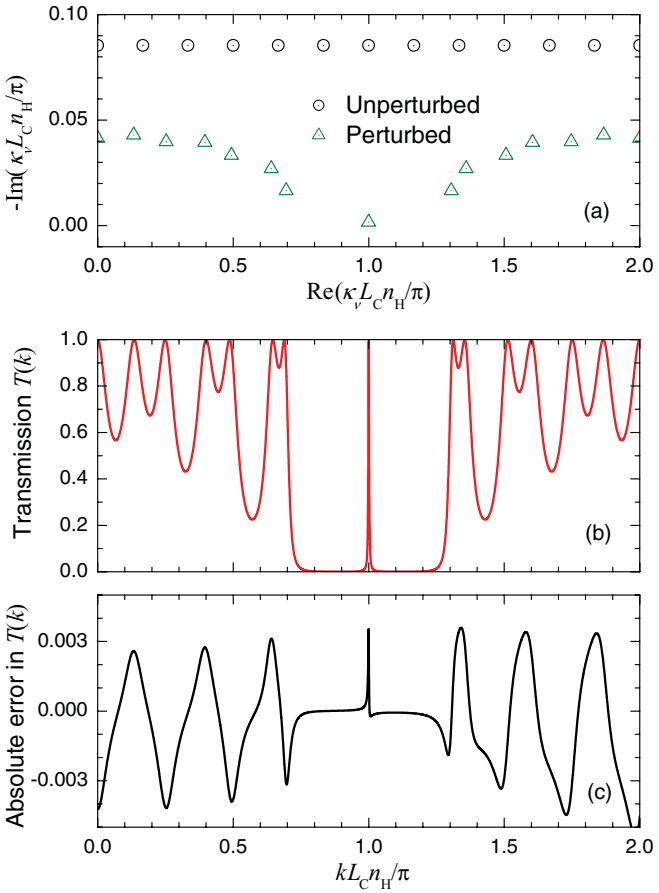

FIG. 16. (Color online) (a) Wave vectors $\varkappa_\nu$ of the resonant states of a microcavity with $P = 3$ pairs of Bragg mirrors on each side calculated via RSE with $N = 801$. (b) Microcavity transmission as a function of the normalized wave vector of the incoming light; L_C and n_C are the cavity thickness and refractive index. (c) The difference in the transmission calculated via RSE and using the scattering-matrix method [22].

optimized for best convergence of the RSE. In order to verify the transmission calculated by the RSE, we use the scattering-matrix method [22], which is a straightforward and precise way of calculating the optical properties of a planar system. Figure 16(c) demonstrates good agreement between the two calculations.

Clearly, there is a one-to-one correspondence between the RS wave vectors in Fig. 16(a) and the MC transmission in Fig. 16(b). Namely, the real part of the wave vectors corresponds to the positions of the peaks in the transmission, while the imaginary part gives their linewidths. This is well understood in view of the spectral representation of the Green's function, Eq. (27), used for the calculation of the transmission via Eq. (29).

One of the modes shown in Fig. 16(a) is rather isolated and has the imaginary part much smaller than the others. This mode, $\varkappa_C$, satisfies the Fabry-Perot resonance condition $\mathrm{Re}\varkappa_C = \pi/(L_C n_C)$ and is called the cavity mode. For the wave vector k of incoming light close to this resonance condition, $k \approx \pi/(L_C n_C)$, the Green's function, Eq. (27), is dominated by a single term corresponding to this narrow mode. As a consequence, there is a sharp peak in the center of a wide stop

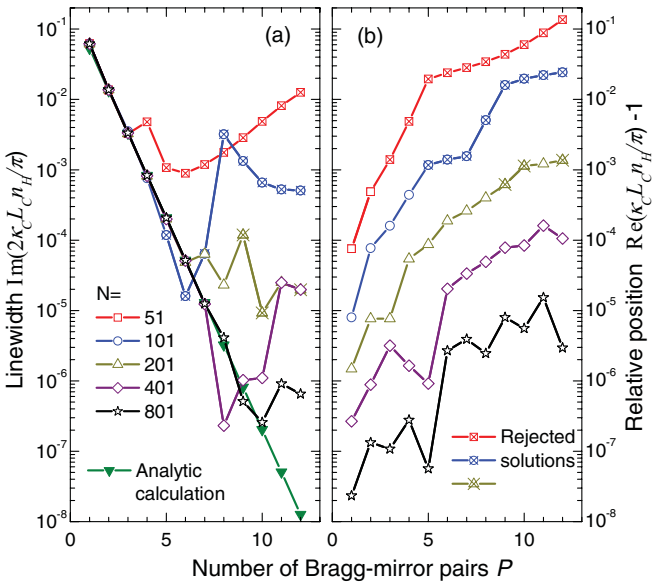

FIG. 17. (Color online) The FWHM (a) and the position of the cavity mode (b) calculated analytically and via the RSE for different number of pairs P of Bragg mirrors on each side of the microcavity. N is the basis size used in the RSE. Where possible, extrapolated wave numbers have been used. Crossed rectangles for $N = 51$ indicate states which are rejected by the SC.

band seen in the transmission in Fig. 16(b). For sufficiently large P an analytic approximation for its full width at half maximum (FWHM) is known as [23,24],

$$\Delta k = \frac{4n_{\text{ext}}}{n_C^2}\left(\frac{n_L}{n_H}\right)^{2P}\frac{1}{L_C + \frac{\lambda_C}{2}\frac{n_L n_H}{n_C(n_H - n_L)}}, \qquad (31)$$

which we use to compare with the RSE calculation. With the refractive index of the external material $n_{\text{ext}} = 1$ and using $\lambda_C = 2L_C$ and $n_C = n_H$, Eq. (31) reduces to $\Delta k = 4(n_H - n_L)(n_L/n_H)^{2P}/(L_C n_H^3)$. A comparison of the above formula with the RSE result for the cavity mode is given in Fig. 17, for different numbers of Bragg-mirror pairs P and for different basis size N in the RSE. Figure 17 demonstrates that the RSE is capable of giving both the correct width and location of sharp resonances in the transmission profile, if a large enough basis is used, in spite of there being no sharp resonances in the basis. As the basis size is enlarged, the width and the peak location of the cavity mode converge to the analytic values. The fact that for a fixed N the cavity mode position and the width are predicted worse for larger P is explained by our choice of the unperturbed slab which always has exactly the same thickness as the Bragg-mirror MC. With the number of Bragg mirrors increasing, the field inside the MC oscillates more rapidly (also shifting the cavity mode toward higher frequencies), which requires a larger number of RSs to be taken into account in order to produce results on the same level of accuracy. We have verified (not shown) that the errors become independent of P, if one and the same constant width of the unperturbed slab is used for different values of P.

The scattering-matrix method (SMM) used in this section for verification of results is considered in the literature as the most suitable method to calculate the optical properties of planar layered structures. The computational time required for calculation of optical spectra using the SMM is proportional to the number of layers times the number of frequency points. In the RSE, the layers are used to calculate the perturbation matrix elements, which determine the RSs. Once the RSs are determined, the GF and/or transmission is generated from the RSs independent of the number of layers. Thus the computational time scales as a weighted sum of the number of layers and the number of frequency points. Consequently, when considering a problem with many layers, such as a smoothly changing dielectric profile or a very complex structure, which exhibits sharp resonances requiring many frequency points, the RSE can be computationally more efficient than the SMM. Furthermore, the RSE directly determines the resonances of the system, without introducing specific scattering geometries and deducing resonances from analytic continuations of the calculated spectra.

V. SUMMARY

The resonant-state expansion has been implemented and validated in planar open optical systems. A reliable method of calculation of resonant states, and in particular their wave numbers, electric fields, as well as the Green's function and the transmission of such systems, has been developed and demonstrated [25]. It provides an estimation of the accuracy and convergency of calculations and an extrapolation of the eigen-wave vectors toward their exact values which are generally not available. Particular examples which illustrate the general method and the developed algorithm include a dielectric slab with wide-layer and δ perturbations as well as an optical microcavity having different number of Bragg mirrors. In these examples, a comparison with exact solutions has been made in order to verify the approach. In all three systems the resonant states and the transmission can be reproduced to any required accuracy by the resonant-state expansion. The wave vectors of resonant states are the most essential part of the calculation as they most strongly affect the optical properties of the system through the poles of the Green's function. The extrapolation of the wave vectors using the power law in the basis size, which has been developed and demonstrated, significantly improve the accuracy of calculations, by one or two orders of magnitude. Application of the method to two- and three-dimensional systems will be reported in future works.

ACKNOWLEDGMENT

M. D. acknowledges support of EPSRC under the DTA scheme.

APPENDIX: ANALYTIC CALCULATION OF RESONANT STATES AND PERTURBATION MATRICES

1. Resonant states of the unperturbed slab

Solving the wave equation (3) with $\Delta\varepsilon(z) = 0$ and the profile of the dielectric constant $\varepsilon(z)$ given by Eq. (10), the electric field of RS n, normalized according to Eq. (5), takes

the form

$$E_n(z) = \begin{cases} (-1)^n A_n e^{-ik_n z}, & z < -a, \\ B_n[e^{i\sqrt{\epsilon_s}k_n z} + (-1)^n e^{-i\sqrt{\epsilon_s}k_n z}], & |z| \leqslant a, \\ A_n e^{ik_n z}, & z > a, \end{cases} \tag{A1}$$

where

$$A_n = \frac{e^{-ik_n a}}{\sqrt{a(\epsilon_s - 1)}}, \quad B_n = \frac{(-i)^n}{2\sqrt{a\epsilon_s}}. \tag{A2}$$

The RS wave vectors are given by

$$k_n = \frac{1}{2a\sqrt{\epsilon_s}}(\pi n - i\,\ln\gamma), \quad n = 0, \pm 1, \pm 2, \ldots, \tag{A3}$$

with

$$\gamma = \frac{\sqrt{\epsilon_s} + 1}{\sqrt{\epsilon_s} - 1}, \tag{A4}$$

all having the same imaginary part.

2. Resonant states of a slab perturbed by a wide dielectric layer

The exact solution of the wave equation (3) for the system with the perturbation given by Eq. (22) and outgoing boundary conditions has the form

$$\mathcal{E}_\nu^{(\mathrm{exact})}(z) = \begin{cases} A_\nu e^{-i\varkappa_\nu z}, & z < -a, \\ B_\nu e^{i\sqrt{\epsilon_s}\varkappa_\nu z} + C_\nu e^{-i\sqrt{\epsilon_s}\varkappa_\nu z}, & -a \leqslant z \leqslant b, \\ D_\nu e^{i\sqrt{\epsilon_p}\varkappa_\nu z} + E_\nu e^{-i\sqrt{\epsilon_p}\varkappa_\nu z}, & b \leqslant z \leqslant a, \\ H_\nu e^{i\varkappa_\nu z}, & z > a, \end{cases} \tag{A5}$$

where $\epsilon_p = \epsilon_s + \Delta\epsilon$, and $b = a/2$. The coefficients in Eq. (A5) are found from the continuity of the electric field and its derivative and the normalization condition (24). The complex-valued RS wave numbers $\varkappa_\nu$ are found by solving a secular equation following from the boundary conditions:

$$\beta\gamma f(k)g(k) - 1 = \frac{\beta - \gamma}{\beta\gamma - 1}[\beta g(k) - \gamma f(k)], \tag{A6}$$

where

$$\beta = \frac{\sqrt{\epsilon_p} + 1}{\sqrt{\epsilon_p} - 1}, \tag{A7}$$

and the functions $f(k)$ and $g(k)$ are defined as

$$f(k) = e^{-2i\sqrt{\epsilon_s}k(a+b)}, \quad g(k) = e^{-2i\sqrt{\epsilon_s}k(a-b)}. \tag{A8}$$

We solve Eq. (A6) using the Newton-Raphson method to find $k = \varkappa_\nu^{(\mathrm{exact})}$.

3. Matrix elements of the wide-layer perturbation

Using Eq. (8) and basis functions (A1) we calculate V_{nm} for the wide-layer perturbation (22) to be

$$\begin{aligned} V_{nm} = \frac{\Delta\epsilon}{\epsilon_s}\frac{1}{4ia\sqrt{\epsilon_s}}[&(-i)^{n+m}\eta(k_n + k_m, z) \\ &+ (-i)^{n-m}\eta(k_n - k_m, z) \\ &+ (-i)^{-n+m}\eta(-k_n + k_m, z) \\ &+ (-i)^{-n-m}\eta(-k_n - k_m, z)]_b^a, \end{aligned} \tag{A9}$$

for $n \neq m$ and

$$V_{nn} = \frac{\Delta\epsilon}{\epsilon_s}\left\{\frac{a-b}{2a} + (-1)^n\frac{[\eta(2k_n, z) + \eta(-2k_n, z)]_b^a}{4ia\sqrt{\epsilon_s}}\right\} \tag{A10}$$

for $n = m$, where $\eta(k, z) = e^{i\sqrt{\epsilon_s}kz}/k$.

4. Resonant states of a slab perturbed by a delta scatterer

In the case of a δ perturbation $\Delta\varepsilon(z) = w\epsilon_d\delta(z - b)$ with $|b| \leqslant a$, the secular equation for the RS wave vectors takes the form

$$[1 + \gamma f(k)][1 + \gamma g(k)] = \frac{2i\sqrt{\epsilon_s}}{w\epsilon_d k}[1 - \gamma^2 f(k)g(k)]. \tag{A11}$$

It is also solved numerically with the help of the Newton-Raphson method to find $k = \varkappa_\nu^{(\mathrm{exact})}$.

5. Matrix elements of the δ perturbation

Using Eq. (8) and basis functions (A1) we calculate V_{nm} for the δ perturbation to be

$$V_{nm} = w\epsilon_d E_n(a/2)E_m(a/2). \tag{A12}$$

[1] E. A. Muljarov, W. Langbein, and R. Zimmermann, Europhys. Lett. **92**, 50010 (2010).
[2] H. M. Lai, P. T. Leung, K. Young, P. W. Barber, and S. C. Hill, Phys. Rev. A **41**, 5187 (1990).
[3] H. M. Lai, C. C. Lam, P. T. Leung, and K. Young, J. Opt. Soc. Am. B **8**, 1962 (1991).
[4] P. T. Leung, S. Y. Liu, S. S. Tong, and K. Young, Phys. Rev. A **49**, 3068 (1994).
[5] P. T. Leung and K. M. Pang, J. Opt. Soc. Am. B **13**, 805 (1996).
[6] K. M. Lee, P. T. Leung, and K. M. Pang, J. Opt. Soc. Am. A **15**, 1383 (1998).
[7] R. Dubertrand, E. Bogomolny, N. Djellali, M. Lebental, and C. Schmit, Phys. Rev. A **77**, 013804 (2008).
[8] G. Gamow, Z. Phys. **51**, 204 (1928); **52**, 510 (1929).
[9] A. J. F. Siegert, Phys. Rev. **56**, 750 (1939).
[10] N. Moiseyev, Phys. Rep. **302**, 212 (1998).
[11] A. Baz', Ya. Zel'dovich, and A. Perelomov, *Scattering, Reactions and Decay in Nonrelativistic Quantum Mechanics* (US Department of Commerce, Washington, DC, 1969).

[12] L. A. Weinstein, *Open Resonators and Open Waveguides* (Golem Press, Boulder, Colorado, 1969).
[13] R. Newton, J. Math. Phys. **1**, 319 (1960).
[14] R. M. More, Phys. Rev. A **4**, 1782 (1971).
[15] A. Taflove and S. C. Hagness, *Computational Electrodynamics: The Finite-Difference Time-Domain Method*, 2nd ed. (Artech House, Norwood, MA, 2000).
[16] S. C. Hagness, D. Rafizadeh, S. T. Ho, and A. Taflove, J. Lightwave Technol. **15**, 2154 (1997).
[17] J. Wiersig, J. Opt. A, Pure Appl. Opt. **5**, 53 (2003).
[18] O. C. Zienkiewicz and R. L. Taylor, *The Finite Element Method*, 5th ed. (Butterworth-Heinemann, Oxford, 2000).
[19] B. M. A. Rahman, F. A. Fernandez, and J. B. Davies, Proc. IEEE **79**, 1442 (1991).
[20] B. N. Jiang, J. Wu, and L. Povinelli, J. Comput. Phys. **125**, 104 (1996).
[21] P. T. Leung and S. T. Ng, J. Phys. A **29**, 141 (1996). We found that the eigenvalue problem (3.16) to be solved suffers from matrix singularities. These can be mitigated to some extent by reformulating the eigenvalue problem in a way not described in the reference.
[22] S. G. Tikhodeev, A. L. Yablonskii, E. A. Muljarov, N. A. Gippius, and T. Ishihara, Phys. Rev. B **66**, 045102 (2002).
[23] L. C. Andreani, Phys. Lett. A **192**, 99 (1994).
[24] V. Savona, L. C. Andreani, P. Schwendimann, and A. Quattropani, Solid State Commun. **93**, 733 (1995).
[25] An executable file calculating RS wave numbers of a planar layered dielectric structure in vacuum is available at http://langsrv.astro.cf.ac.uk/RSE/RSE.html.